Large-amplitude monochromatic ULF waves detected by Kaguya at the Moon

Tomoko Nakagawa,[1] Akihito Nakayama,[1] Futoshi Takahashi,[2] Hideo Tsunakawa,[2] Hidetoshi Shibuya,[3] Hisayoshi Shimizu,[4] and Masaki Matsushima[2]

Received 11 October 2011; revised 7 January 2012; accepted 3 February 2012; published 3 April 2012.

[1] Large amplitude, monochromatic ultra low frequency (ULF) waves were detected by MAP/LMAG magnetometer onboard Kaguya during the period from 1 January 2008 to 30 November 2008 on its orbit 100 km above the lunar surface. The dominant frequency was $8.3 \times 10^{-3} - 1.0 \times 10^{-2}$ Hz, corresponding to the periods of 120 s – 100 s. The amplitude was as large as 3 nT. They were observed in 10% of the time when the moon was in the solar wind far upstream of the Earth's bow shock. They were detected only by Kaguya on the orbit around the moon, but not by ACE in the upstream solar wind. The occurrence rate was high above the terminator and on the dayside surface. The direction of the propagation was not exactly parallel to the interplanetary magnetic field, but showed a preference to the direction of the magnetic field and the direction perpendicular to the surface of the moon below the spacecraft. The sense of rotation of the magnetic field was left-handed with respect to the magnetic field in 53% of the events, while 47% showed right-handed polarization. The possible generation mechanism is the cyclotron resonance of the magnetohydrodynamic waves with the solar wind protons reflected by the moon. The energy of the reflected protons can account for the energy of the ULF waves. The propagation direction which are not parallel to the incident solar wind flow can explain the observed frequency and the nearly equal percentages of the left-handed and right-handed polarizations.

Citation: Nakagawa, T., A. Nakayama, F. Takahashi, H. Tsunakawa, H. Shibuya, H. Shimizu, and M. Matsushima (2012), Large-amplitude monochromatic ULF waves detected by Kaguya at the Moon, *J. Geophys. Res.*, *117*, A04101, doi:10.1029/2011JA017249.

1. Introduction

[2] The solar wind interaction with the moon is quite different from that with the Earth. Because of the absence of the global magnetic field and the atmosphere, the solar wind particles hit the lunar surface directly. They are absorbed by the lunar surface, creating a plasma cavity called the lunar wake, on the downstream side of the moon [*Lyon et al.*, 1967; *Ness et al.*, 1968; *Schubert and Lichtenstein*, 1974].

[3] Since it was believed that all the solar wind particles were absorbed by the lunar surface, the solar wind interaction with the moon was studied in terms of the lunar wake [*Colburn et al.*, 1967; *Russell and Lichtenstein*, 1975; *Owen et al.*, 1996; *Ogilvie et al.*, 1996; *Bosqued et al.*, 1996; *Kellogg et al.*, 1996; *Lin et al.*, 1998; *Futaana et al.*, 2001; *Halekas et al.*, 2005] or the surface charging [*Lindeman et al.*, 1973; *Freeman et al.*, 1973; *Freeman and Ibrahim*, 1975; *Halekas et al.*, 2002, 2003, 2008; *Colwell et al.*, 2007]. There were some reports on the wave activities around the moon, such as the monochromatic whistler waves detected by WIND [*Farrell et al.*, 1996] or GEOTAIL [*Nakagawa et al.*, 2003]. Their generation was attributed to the lunar wake because they were detected when the spacecraft were magnetically connected with the lunar wake. Similar low-frequency waves were also observed by Lunar Prospector [*Halekas et al.*, 2006b; *Lin et al.*, 1998], and were interpreted in association with the lunar external magnetic enhancements [*Halekas et al.*, 2006a] or the lunar crustal magnetic field.

[4] In 2008, the Japanese lunar explorer Kaguya discovered reflection of the solar wind protons at the lunar surface [*Saito et al.*, 2008, 2010]. Kaguya detected as much as 0.1 – 1% of the incident solar wind protons coming from the lunar surface when the spacecraft was on the dayside of the moon. They were not specularly reflected but rather backscattered at the lunar surface or magnetically reflected by the crustal magnetic field. Some of the protons were further accelerated by the electric field induced by the solar wind convection. As a result, the angular distribution of the reflected protons was much broader than that of the incident solar wind protons. The reports on the solar wind proton reflection by the moon were followed by the Kaguya detection of the protons once scattered and then

[1]Information and Communication Engineering, Tohoku Institute of Technology, Miyagi, Japan.
[2]Department of Earth and Planetary Sciences, Tokyo Institute of Technology, Tokyo, Japan.
[3]Department of Earth and Environmental Sciences, Kumamoto University, Kumamoto, Japan.
[4]Earthquake Research Institute, University of Tokyo, Tokyo, Japan.

0148-0227/12/2011JA017249

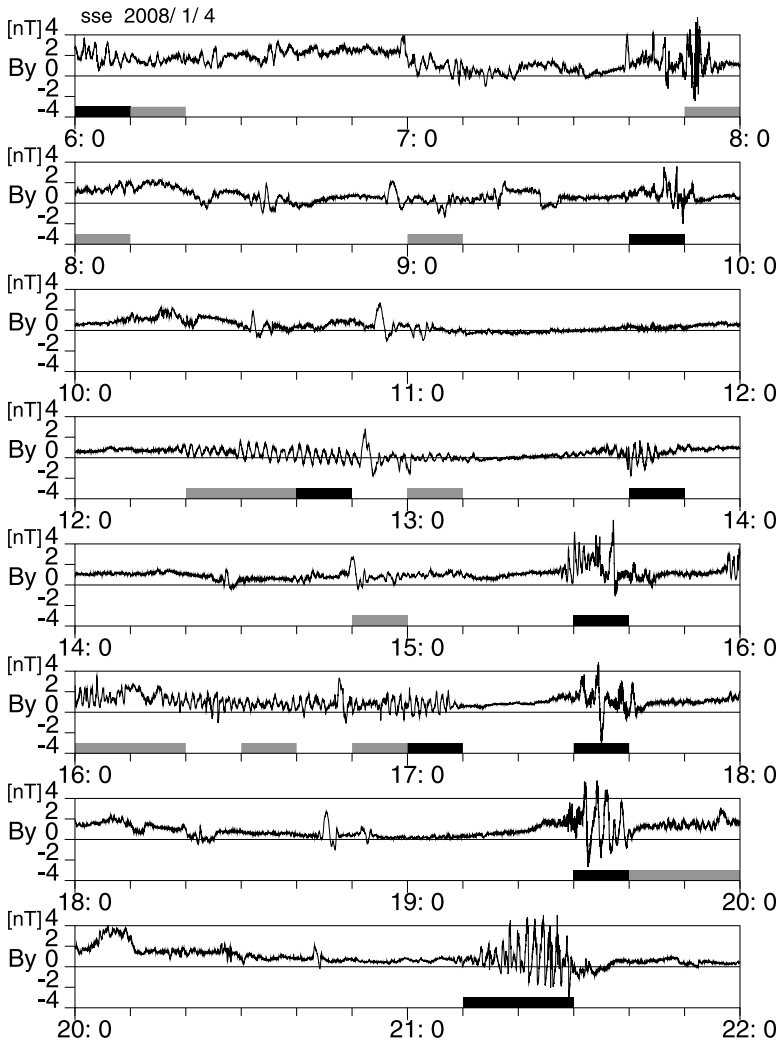

Figure 1. A 16-hour plot of a magnetic field component B_y in SSE coordinate system observed by Kaguya during the period from 6:00 to 22:00 on 4 January 2008 at an altitude of 100 km above the terminator of the moon. The orbit on this day will be presented in Figure 3. Bars at the bottom of each panel indicate 10 minute periods during which the monochromatic ULF waves were detected according to the criteria which will be described in section 3.1. Black and gray bars are for large-amplitude waves (with power density greater than 100 nT^2/Hz) and small-amplitude waves (with power density of 10–100 nT^2/Hz), respectively.

picked-up by the solar wind motional electric field to get into the deepest lunar wake [*Nishino et al.*, 2009], the Chang'E-1 observation of picked-up protons at the lunar terminator [*Wang et al.*, 2010], and Chandrayaan-1 observations of proton reflection at the magnetic anomalies [*Lue et al.*, 2011]. Prior to Kaguya observation, *Futaana et al.* [2003] reported Nozomi detection of the nonthermal protons originating from the dayside surface of the moon.

[5] Kaguya also observed enhancements of the magnetic fluctuations above the dayside surface of the moon or above the lunar terminator while the moon was exposed to the solar wind stream. Most commonly observed were large-amplitude, nearly monochromatic low frequency waves of 0.01 Hz [*Tsunakawa et al.*, 2010], and higher frequency, non-monochromatic fluctuations within the frequency range from 0.03 to 10 Hz [*Nakagawa et al.*, 2011].

[6] Predominance of the two frequency bands is analogous to the low-frequency waves in the upstream of the Earth's bow shock [*e.g.*, *Fairfield*, 1969, 1974; *Hoppe et al.*, 1981; *Russell*, 1994a, 1994b]. The low-frequency waves with periods near 50 s and 1 s are thought to be the magnetohydrodynamic (MHD) waves [*Fairfield*, 1969] and the whistler waves [*Fairfield*, 1974], respectively, generated through the resonant interaction with the ions reflected by the Earth's bow shock. It is likely that the two frequency bands detected by Kaguya were also generated by the solar wind protons reflected by the moon. If it is the case, this is a new kind of solar wind interaction with the moon that had not been known. *Nakagawa et al.* [2011] explained the non-monochromatic waves of 0.03 – 10 Hz as the whistler waves excited through the cyclotron resonance with the solar wind protons reflected by the moon. Here in this paper, we concentrate on the large-amplitude, low-frequency waves with the period near 100 s. First, we show the

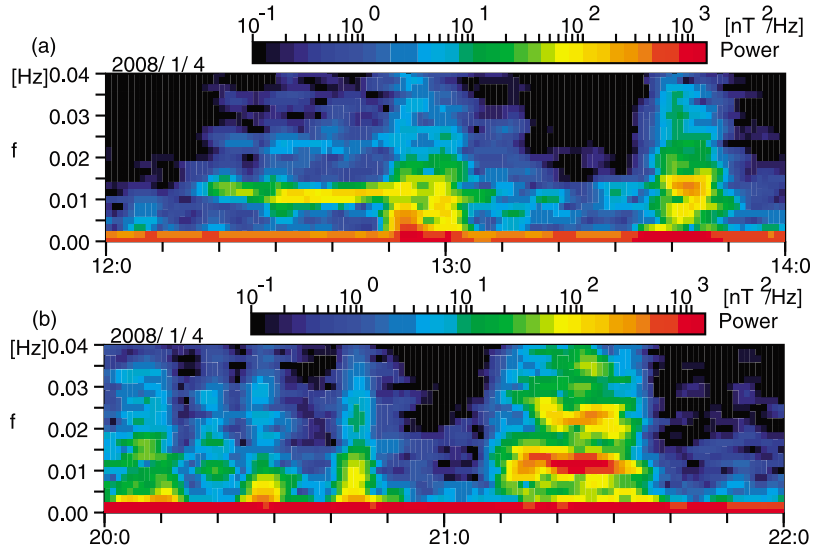

Figure 2. Examples of the dynamic spectra of the magnetic fluctuations observed by Kaguya during the periods from (a) 12:00 to 14:00 and (b) 20:00 to 22:00 on 4 January 2008. To gain temporal resolution, Fourier transform of 1-sec averaged magnetic field data was carried out sliding a 600 s Humming window by 60 s. The spectra thus obtained were displayed on the center of each 600 s period.

occurrence properties of the 100 s waves and then examine how their generation can be explained by the cyclotron resonance with the reflected protons.

2. Observations

[7] The magnetic field data used in this study were obtained by MAP/LMAG magnetometer onboard Kaguya [*Shimizu et al.*, 2008; *Takahashi et al.*, 2009; *Tsunakawa et al.*, 2010] during the period from 1 January 2008 to 30 November 2008. The spacecraft was on its polar orbit encircling the moon every 118 min at an altitude of 100 km. The magnetic field vectors were obtained with sampling frequency of 32 Hz and were averaged over 1 s. The magnetic field data obtained by Kaguya in the solar wind were consistent with those obtained by ACE [*Tsunakawa et al.*, 2010].

[8] Figure 1 is a 16-hour plot of a magnetic field component B_y in Selenocentric Solar Ecliptic (SSE) coordinates obtained by Kaguya on 4 January 2008 above the lunar terminator in the unperturbed solar wind. Large amplitude, low frequency waves were significant from the beginning of the period displayed, and they became almost purely monochromatic at 12:20 UT. The oscillation period was nearly 100 s. The monochromatic wave persisted for nearly 30 min, followed by a typical waveform observed recurrently every 2 hours, which may be the lunar external magnetic enhancements associated with a crustal magnetic field [*Halekas et al.*, 2006a]. The amplitude of the monochromatic wave once depressed, and re-appeared at 15:57 until 17:08, after some short enhancements around 13:00, 13:40, 14:50, and 15:30. The largest amplitude was observed around 19:32 and 21:25, when the spacecraft was located on the southern hemisphere. Black and gray bars at the bottom of each panel indicate the periods of large- and small-amplitude monochromatic ULF waves, respectively, whose detection criteria will be explained in section 3.1.

[9] Figure 2 shows examples of the dynamic spectra for the periods selected from Figure 1. Enhancements of the power of the frequency around 0.012 Hz are significant during the periods from 12:18 to 12:55, and from 21:12 to 21:32. The power density was about 10 nT^2/Hz for 12:18 – 12:30, 10^2 nT^2/Hz for 12:30 – 12:55, and as much as 10^3 nT^2/Hz for 21:17 – 21:27.

[10] Figure 3 shows the orbit of Kaguya in Geocentric Solar Ecliptic (GSE) coordinates (Figure 3a) and in SSE coordinates (Figures 3b–3d) on the same day. The moon, going around the Earth at 60 Earth radii (R_E), was far upstream from the Earth's bow shock and from the nominal position of the ion foreshock which is the region characterized by ULF waves produced by the backstreaming ions reflected by the Earth's bow shock [*Greenstadt et al.*, 1995; *Le and Russell*, 1992]. It is not likely that the large amplitude waves shown in Figure 1 were originating from the Earth's bow shock, because the shock-related waves were attenuated due to the large distance. On the basis of the ISEE-3 and GEOTAIL observations at the GSE-x coordinate between −50 and 15 R_E, *Sugiyama et al.* [1995] showed an empirical relationship of the normalized amplitude of the shock-related wave in the form of $A\exp(X_s/L_X - D/L_D)$ with $L_X = 62 \pm 12$ R_E, $L_D = 59 \pm 38$ R_E and $A = 0.37 \pm 0.04$, where X_s is the x component of the position of the shock foot point of the interplanetary magnetic field, and D is the distance from the bow shock measured along the magnetic field line. On 4 January 2008, the distance D was typically around 50 R_E and X_s was about 8 R_E, and we obtain a rough estimation of the normalized amplitude of the shock-related wave of 0.2. Since the magnitude of the magnetic field was about 3 nT between 21:10 and 21:30, the amplitude of the shock-related wave would be about 0.6 nT. This is much smaller than the observed amplitude of 3 nT. Figures 3b–3d show that Kaguya was encircling the moon on the orbit above the terminator. It should be noted that the low frequency waves were detected on the farther side of the moon from the Earth's bow shock.

[11] The 100 s oscillation was not present in the upstream solar wind. Figure 4 compares Kaguya observation (black curves) with the upstream solar wind magnetic field observed by ACE (gray curves) shifted to the Kaguya position by the

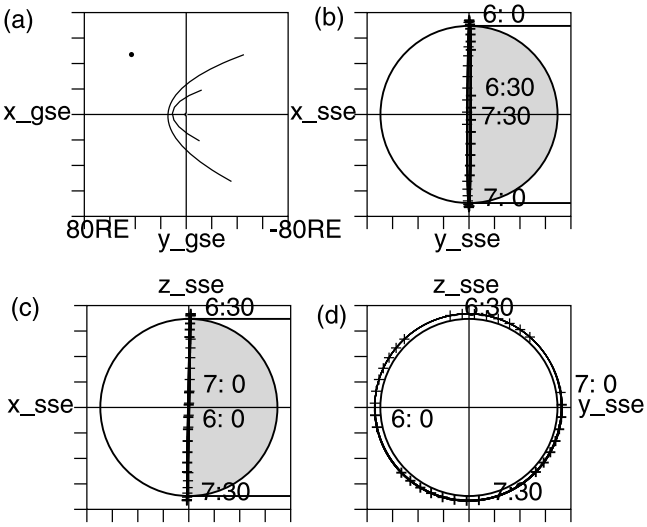

Figure 3. The orbit of Kaguya on 4 January 2008 (a) with respect to the Earth, magnetopause, and the bow shock displayed in GSE coordinates, and with respect to the moon in (b) *x-y*, (c) *x-z*, and (d) *y-z* planes in SSE coordinates. Kaguya was encircling the moon at an altitude of 100 km with orbital period of about 118 min.

time for the solar wind to travel the distance between the two spacecraft. The position of ACE was (13.9, −0.5, 1.5) × 10^5 km and the position of Kaguya was (3.1, −2.6, −0.4) × 10^5 km in the Geocentric Solar Ecliptic (GSE) coordinate system, and the time delay for the solar wind of 300 km/s was about 1 hour. No signature of 100 s oscillation was found in ACE magnetic field data in Figure 4, indicating that the magnetic oscillation was associated with the moon.

[12] The 100 s oscillation is also recognized in the magnitude of the magnetic field in Figure 4. That is, the wave had a compressional component. Color bars at the bottom of Figure 4 indicate the magnetic connection of the spacecraft to the lunar surface. The largest oscillation was detected during the period when the spacecraft was magnetically connected with the lunar surface.

3. Occurrence Property

3.1. Dominant Frequency

[13] Figure 5 is an example of the spectrum of the magnetic fluctuations for the period from 21:17 to 21:27 on 4 January 2008, selected from Figure 4. Black and gray curves are for the magnetic components of maximum and intermediate variance directions, respectively. Both curves have clear peaks at 0.012 Hz. The vertical line indicates the local proton cyclotron frequency, 0.039 Hz, calculated from the magnitude 2.6 nT of the average magnetic field (−2.2, 1.2, 0.5) nT. The peak frequency was much lower than the proton cyclotron frequency.

[14] Similar events were searched in the Kaguya magnetic field data obtained in the solar wind unperturbed by the presence of the Earth's bow shock. To avoid wave activities originating from the bow shock, we limit the area of observation to $x_{gse} > 0$, where x_{gse} is the Kaguya position with respect to the Earth in GSE coordinates. It is equivalent to the distance more than 27 R_E from the nominal position of the bow shock.

[15] The 3 components of the Kaguya 1-s magnetic field data were Fourier-transformed for every 600 s period after application of the Hamming window. Detection of the monochromatic ULF waves in the present study is defined by the following criteria: (1) the sum of the power of the 3 components of the magnetic variation of a frequency is more than 3 times larger than that of the next lower frequency, and (2) the

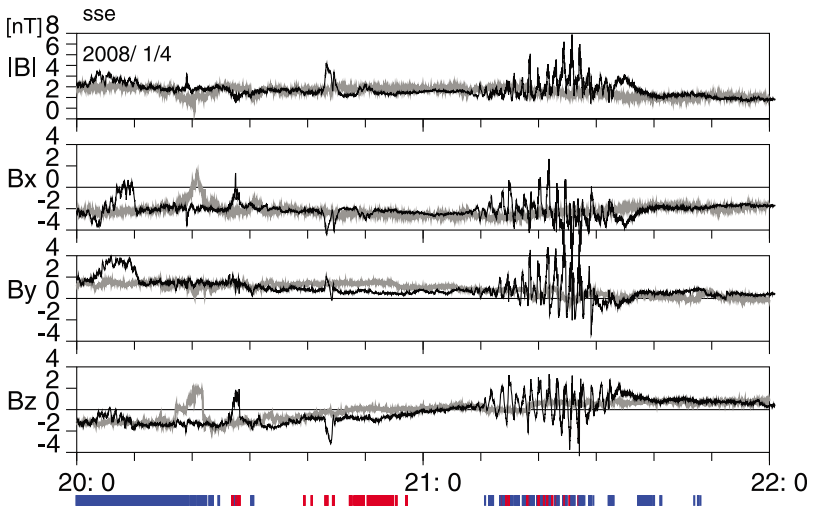

Figure 4. The 1-s averages of the magnetic field observed by Kaguya (black) in SSE coordinate system compared with the 1-s averages of the solar wind magnetic field observed by ACE (gray) at (13.9, −0.5, 1.5) × 10^5 km in GSE coordinates, shifted to the Kaguya position (3.1, −2.6, −0.4) × 10^5 km. To compare the waveforms, the time shift was fixed to 1 hour for the solar wind to travel the distance between the two spacecraft at the solar wind speed of 300 km/s. ACE data are in GSE coordinates, but the difference between SSE and GSE is negligible. The 100 s period oscillation is observed only in Kaguya data. The blue and red bars at the bottom of the magnetogram indicate the magnetic connection of the spacecraft to the nightside and dayside surface of the moon, respectively.

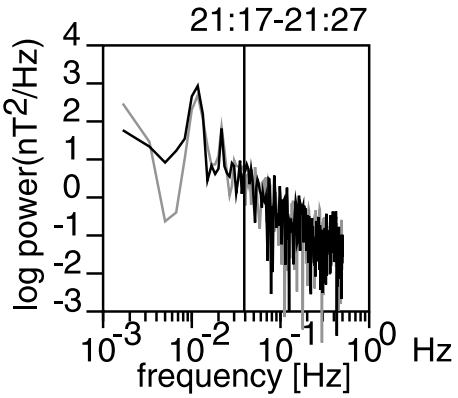

Figure 5. The spectrum of the magnetic fluctuations observed by Kaguya during the 10 minute period from 21:17 to 21:27 on 4 January 2008. Curves are for the magnetic components of maximum (black) and intermediate (gray) variances, respectively. The directions of maximum and intermediate variances are calculated by minimum variance analysis [*Sonnerup and Cahill*, 1967]. The vertical line indicates the proton cyclotron frequency for this period.

power of the frequency is higher than 100 nT^2/Hz. The spectral property of the power density of the solar wind magnetic fluctuations of this frequency range is characterized with $f^{-1.5} - f^{-1.7}$ [*e.g., Bruno and Carbone*, 2005, and references therein], and the ratio of the power of the higher frequency to that of the lower frequency should be smaller than unity. In the present study, we use the ratio 3 as the criterion to avoid temporal fluctuations of the spectrum. The second criterion was set to avoid too small variations at high frequencies, but it tends to restrict the detection of the events to lower frequency, so we also tried another criterion of 10 nT^2/Hz to investigate the distribution of the dominant frequency of the ULF waves. Representative examples of the waveforms of 10 nT^2/Hz and 100 nT^2/Hz are seen in Figure 1 at 12:20–12:40 and 21:10–21:30, respectively. In Figure 1, gray bars indicate the periods of the monochromatic ULF waves with power density of 10–100 nT^2/Hz, and black bars indicate those with power density greater than 100 nT^2/Hz.

[16] Using the criteria, we detected the high-power (>100 nT^2/Hz) monochromatic ULF waves in 10% of the 22916 periods analyzed. When we relaxed the second criterion to be 10 nT^2/Hz, the occurrence frequency rose up to 47%. It indicates that the monochromatic ULF waves are common phenomena on the orbit around the moon in the solar wind.

[17] Figure 6 shows the distribution of the peak frequency of the ULF waves. They were most frequently observed at $8.3 \times 10^{-3} - 1.0 \times 10^{-2}$ Hz, corresponding to the periods of 120 s – 100 s. The distribution of the large amplitude events (Figure 6a) is only slightly shifted to lower frequency than that of the events detected with the criterion >10 nT^2/Hz (Figure 6b).

3.2. Site of Detection

[18] Figure 7 is a map of detection of the monochromatic ULF waves in SSE coordinate system, colored by the occurrence probability of the events with power density greater than 10 nT^2/Hz. To produce the map, we carried out the Fourier transform by sliding the 600 s window by 10 s, because the spacecraft moves as much as 30° in latitude within the 600 s period due to the orbital motion. Figure 7 shows that the occurrence rate was high in the longitudes between −100° and 100°, above the terminator and on the dayside of the moon. The occurrence rate was more than 80% above the terminator in the longitudes −90° ± 30° and 90° ± 30°. It was much higher than that of the subsolar point at the longitude of 0°.

[19] Figure 8 is the map of the selenographic distribution of the occurrence probability of the monochromatic ULF waves in the Mean Earth/Polar Axis (ME) reference system. The prime meridian (0° longitude) is defined by the mean Earth direction, and the area between 90° and 270° in longitude corresponds to the far side of the moon [*LRO Project and LGCWG*, 2008]. High occurrence rate is observed at around 180° in longitude and −45° in latitude, near the magnetic anomalies at Imbrium antipode and Serenitatis antipode [*Tsunakawa et al.*, 2010; *Richmond and Hood*, 2008; *Mitchell et al.*, 2008; *Purucker and Nicholas*, 2010].

3.3. Direction of Propagation

[20] The minimum variance analysis [*Sonnerup and Cahill*, 1967] was applied to each 600 s period to obtain the direction of the wave number vector **k** of the ULF waves. Figure 9 shows an example of the minimum variance direction for the same period from 21:17 to 21:27 on 4 January 2008 as in Figure 5. The minimum variance direction, (−0.64, 0.06, 0.77) in SSE coordinates, was obtained with a good accuracy, indicated by the ratio 2.2 of the intermediate to minimum variance [*Lepping and Behannon*, 1980]. The minimum variance direction was not parallel to the background magnetic field, consistently with the compressional component as seen in Figure 4. The angle between them was 44°.

[21] Figure 10 shows the distribution of the direction of the **k** vector obtained by the minimum variance analysis for 396652 periods for which the ratio of the intermediate to minimum variance was greater than 2. Although the **k** vectors

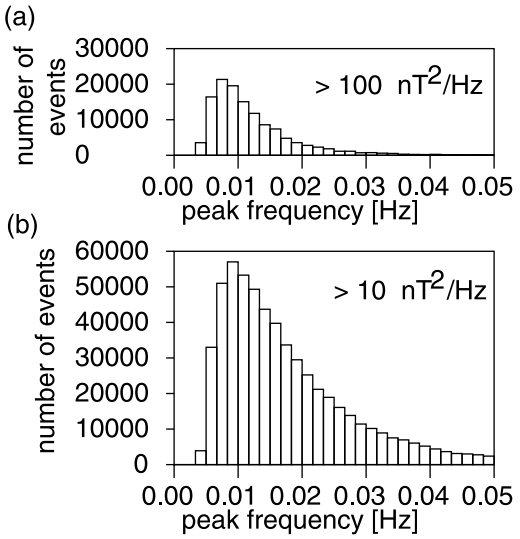

Figure 6. Distribution of the peak frequency of the monochromatic ULF waves detected by Kaguya on its orbit at an altitude of 100km above the moon, during the period from 4 January 2008 to 30 November 2008. Events whose power density at the dominant frequency was more than (a) 100 nT^2/Hz, and (b) 10 nT^2/Hz.

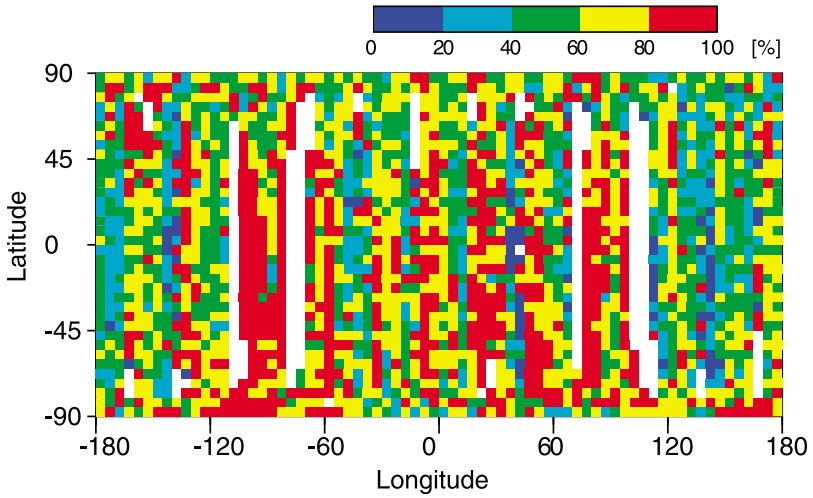

Figure 7. Distribution of the monochromatic ULF waves with power density greater than 10 nT^2/Hz in SSE coordinate system, colored by the occurrence probability. The area of the longitude between −90° and 90° is the dayside surface of the moon. The subsolar point corresponds to the longitude of 0° and the latitude of 0°. Blank areas indicate no observations.

were distributed over a wide range of directions, Figure 10a shows a significant preference to −45° in longitude, in the direction of the average solar wind magnetic field. In Figure 10b we recognize a concentration on −60° in latitude, which suggests an association with the largest magnetic anomalies.

[22] Figure 11 shows the distribution of the angles between the **k** vector and (a) the background magnetic field of each 600 s period, (b) the *x*-axis of the SSE coordinate system as an approximate direction of the solar wind flow, and (c) the vector normal to the lunar surface just below the position of the spacecraft. The number of events is divided by the solid angle of each range. The **k** vectors tend to make small angle from the background magnetic field, but not exactly parallel to it. The **k** vectors show no preferred angle with respect to the solar wind flow, but show a significant preference to small angles with respect to the normal to the lunar surface. Figure 11 shows the angular distribution of **k** vectors of left-hand and right-hand polarized waves separately, but no difference was found between them. It should be noted that the minimum variance analysis cannot distinguish parallel and antiparallel directions.

[23] An attempt was made to find a possible relationship between the direction of the **k** vector and the position of the spacecraft. The minimum variance directions were averaged over each 5° bins of longitudes and latitudes of the observation sites in the SSE coordinate system. Because the minimum variance analysis gives a direction vector but no information of orientation, we averaged the directions on the assumption that they were directed outward from the moon. Figure 12a shows the direction of the **k** vectors averaged over 5° range of the latitudes on the noon-midnight meridian in the longitudes 0° ± 60° (dayside) and 180° ± 60° (nightside). The **k** vectors were directed northward in the northern hemisphere, while they were directed southward when the spacecraft was in the

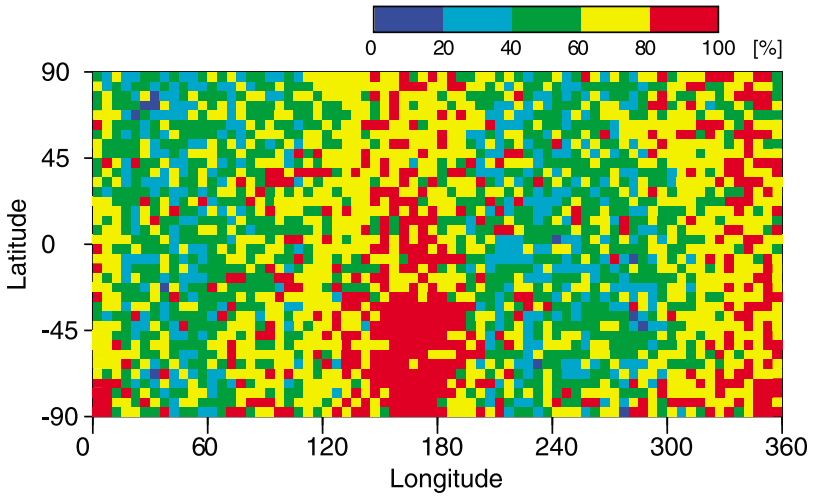

Figure 8. Selenographic distribution of the monochromatic ULF waves colored by the occurrence probability in ME coordinate system. The prime meridian (0° longitude) is defined by the mean Earth direction. The area between 90° and 270° in longitude corresponds to the far side of the moon.

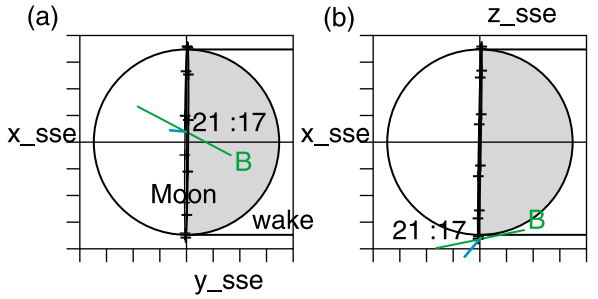

Figure 9. An example of the minimum variance direction (blue bars) together with the average magnetic field (green lines) for the periods from 21:17–21:27 on 4 January 2008, plotted on the position of Kaguya at the time of the observation. Projections onto the (a) *x-y* and (b) *x-z* planes of the SSE coordinate system.

southern hemisphere (on the assumption that they were oriented outward from the moon). Figure 12b shows the results for the dawn-dusk meridian obtained in the longitudes $-90° \pm 30°$ (dawnside), and $90° \pm 30°$ (duskside). The **k** vectors tend to be perpendicular to the lunar surface, consistently with what we have seen in Figure 11c. Figure 12c is an azimuthal plot of the averaged direction of the **k** vectors obtained within 30° from the ecliptic plane. Again the **k** vectors were directed nearly perpendicular to the lunar surface. The absence of the **k** vectors in some longitudes is due to the lack of observation, the smallness of the number of events in the duskside equator, or the inaccuracy of the direction of the **k** vectors. It should also be noted in Figures 12a and 12c that the **k** vectors on the terminator were slightly tilted to the sunward direction.

3.4. Sense of Rotation

[24] Figure 13 shows two examples of the hodograms of the magnetic field variation of the ULF waves, in which the background magnetic field is directed to the reader. During the period from 21:22:00 to 21:25:20 on 4 January 2008 (Figure 13a), the tip of the magnetic field vector rotated clockwise, showing left-hand polarization with respect to the background magnetic field. Only several minutes later, during the period from 21:30:00 to 21:32:00 (Figure 13b), the magnetic field began to rotate in the opposite direction according as the minimum variance direction varied from (−0.64, 0.06, 0.77) to (−0.37, 0.89, 0.27).

[25] Figure 14 shows the observed sense of rotation of the magnetic field with respect to the background magnetic field for the same periods as displayed in Figure 2. The intense monochromatic ULF wave as observed from 12:18 to 12:55 in Figure 2 was dominated by left-handed polarization indicated with blue color in Figure 14a. The most intense monochromatic ULF wave starting from 21:12 at 0.012 Hz is dominated by left-handed polarization (blue) until 21:27 (as the central time of the 600 s period), then the polarization turned to be right-handed (red) at 21:32 (Figure 14b).

[26] Investigation of all the 396652 events whose **k** vectors were obtained with significant accuracy revealed that 53% of the events were left-hand polarized and 47% were right-handed. This makes contrast with the upstream waves at the Earth's bow shock dominated by left-hand polarization [*Fairfield*, 1969]. The possible explanation for the difference will be given in 5. Discussion.

4. Generation Mechanism

4.1. Summary of Observations

[27] The properties of the magnetic fluctuations are summarized as follows:

[28] 1. Large-amplitude, monochromatic ULF waves were found in the solar wind magnetic field around the moon on the orbit of 100 km above the lunar surface when the moon was exposed to the solar wind far upstream of the Earth's bow shock.

[29] 2. They were not detected in the upstream solar wind magnetic field.

[30] 3. The dominant frequency was typically 0.01 Hz.

[31] 4. The occurrence rate was 10% for large amplitude events and 47% for smaller events.

[32] 5. The occurrence rate was high above the terminator and on the dayside of the moon.

[33] 6. The occurrence rate was high in the southern hemisphere of the far side of the moon.

[34] 7. The magnetic field variation had the compressional component.

[35] 8. The wave number vectors were not exactly parallel to the background magnetic field, but they showed a preference to the direction of the magnetic field and the direction perpendicular to the surface of the moon.

[36] 9. Both left-hand and right-hand polarizations were almost equally observed.

4.2. Resonance With the Reflected Protons

[37] The monochromatic nature of the ULF waves suggests that they were generated through a resonant interaction. The detection of the ULF waves on the dayside of the moon, and the predominance above the magnetic anomalies suggest that the waves were associated with the solar wind particles reflected by the moon, in analogous to the upstream waves generated by the solar wind protons reflected by the Earth's bow shock [*Fairfield*, 1969]. Here we discuss the wave

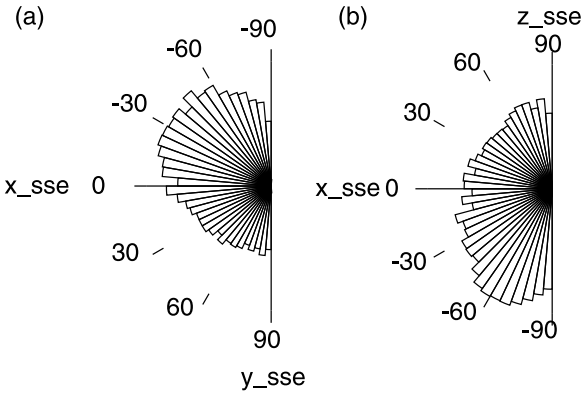

Figure 10. Distribution of the direction of the **k** vector obtained by the minimum variance analysis for 396652 periods for which the ratio of the intermediate to minimum variance was greater than 2. (a) Distribution in the ecliptic plane. (b) Distribution in a meridional plane. The number of events is divided by the solid angle of each latitudinal range.

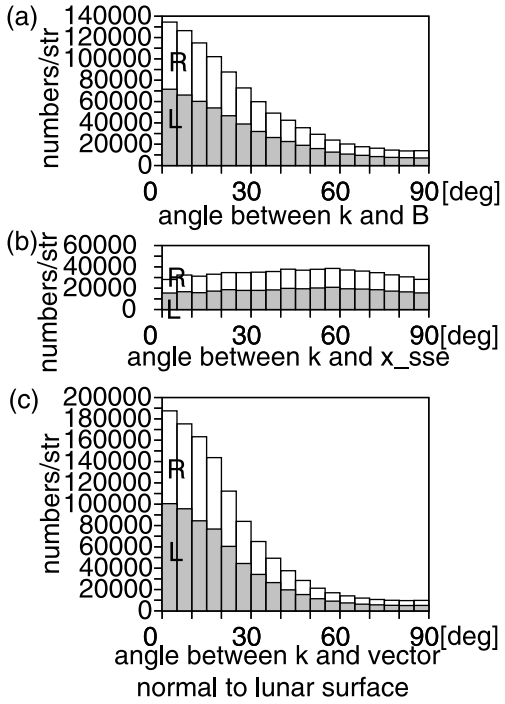

Figure 11. The distribution of the angle between the **k** vector and (a) the background magnetic field, (b) the *x*-axis of the SSE coordinate system as an approximate direction of the solar wind flow, and (c) the vector normal to the lunar surface just below the position of the spacecraft. The letters L and R indicate the left-handed and right-handed polarization with respect to the background magnetic field, respectively.

excitation through a cyclotron resonance with the protons reflected by the moon.

[38] A wave with an angular frequency ω and a wave number vector **k** propagating in a solar wind plasma is detected by a spacecraft at the angular frequency

$$\omega'_{sc} = \omega + \mathbf{k} \cdot \mathbf{V}_{sw}, \tag{1}$$

where $\mathbf{V}_{sw}$ is the bulk velocity of the solar wind flow. The sense of polarization observed from the spacecraft depends on the direction of the background magnetic field $\mathbf{B}_0$ and the chirality h of the magnetic field, which is defined as

$$\begin{cases} b_x &= B_\perp \cos(kz - \omega t) \\ b_y &= hB_\perp \sin(kz - \omega t) \end{cases} \tag{2}$$

on the assumption that the magnetic field **B** is the sum of the constant field $\mathbf{B}_0$ and the wave component $\mathbf{b} = (b_x, b_y, 0)$ in a coordinate system whose z axis is parallel to the wave number vector **k** for simplicity. Here we assume a circularly polarized wave with an amplitude $B_\perp$. Figure 15 illustrates the direction of rotation of the wave component **b**. Positive h gives an anti-parallel type helix for which $\nabla \times \mathbf{b}$ is in the direction opposite to **b** for positive k, while negative h gives a parallel type helix with $\nabla \times \mathbf{b}$ in the same direction as **b**. Hereafter we assume positive k, because the configuration of negative k can be given by that of positive k with reversed h. If we assume positive ω together with positive k, the rotation of the magnetic field at a fixed position in the solar wind frame is left-handed with respect to the z axis for positive h, while it is right-handed for negative h. For the case where $\mathbf{B}_0 \cdot \mathbf{k}$ is positive, the positive h gives left-handed polarization with respect to the magnetic field. The sense of rotation reverses for negative h, negative ω and for negative $\mathbf{B}_0 \cdot \mathbf{k}$.

[39] Observed from a spacecraft, the wave is detected as left-handed if $\omega'_{sc} h \mathbf{B}_0 \cdot \mathbf{k}$ is positive. By taking positive value of the observed angular frequency ω_{obs} for left-hand polarization with respect to $\mathbf{B}_0$, we have

$$\sigma \omega'_{sc} = \omega_{obs}, \tag{3}$$

where $\sigma = 1$ for positive $h\mathbf{B}_0 \cdot \mathbf{k}$ (anti-parallel type helix with $\mathbf{B}_0 \cdot \mathbf{k} > 0$, or parallel type helix with $\mathbf{B}_0 \cdot \mathbf{k} < 0$) and $\sigma = -1$ for negative $h\mathbf{B}_0 \cdot \mathbf{k}$.

[40] The reflected protons with the velocity $\mathbf{V}_p$ would observe the wave at the angular frequency further Doppler-shifted to

$$\omega'_p = \omega + \mathbf{k} \cdot \mathbf{V}_{sw} - \mathbf{k} \cdot \mathbf{V}_p, \tag{4}$$

that is,

$$\omega'_p = \omega'_{sc} - \mathbf{k} \cdot \mathbf{V}_p. \tag{5}$$

It should be noted that the velocity distribution of the reflected protons was not a field aligned beam, but the angular distribution was broad [*Saito et al.*, 2010]. *Saito et al.* [2010, Figure 25] schematically illustrates the orbits of the solar wind protons backscattered at the lunar surface, or reflected by the magnetic anomalies. The broad angular distribution of the reflected protons suggests that they have significant velocity components perpendicular to the magnetic field. Such velocity distribution is likely to be unstable to the cyclotron resonance.

[41] The condition for the cyclotron resonance between the wave and the reflected protons is that the sense of rotation of the electric and the magnetic fields as seen from the protons are left-handed with respect to the background magnetic field, and

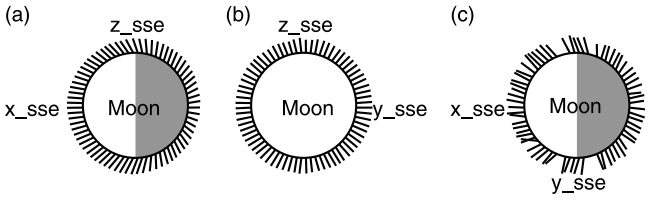

Figure 12. Direction of the **k** vectors averaged for each $5^\circ \times 5^\circ$ bins of location of the spacecraft in the SSE coordinate system. (a) Latitude dependence of 296111 **k** vectors obtained on the noon-midnight meridian in which the longitude ϕ_{sc} was in the range $-60^\circ < \phi_{sc} < 60^\circ$ (dayside), $-180^\circ < \phi_{sc} < -120^\circ$ (nightside), and $120^\circ < \phi_{sc} < 180^\circ$ (nightside). At least 2984 **k** vectors were used for the average of each bin. (b) Latitude dependence of 100541 **k** vectors above the terminator for the range $-120^\circ < \phi_{sc} < -60^\circ$ (dawnside) or $60^\circ < \phi_{sc} < 120^\circ$ (duskside). At least 815 **k** vectors were used for the average of each bin. (c) Azimuthal distribution of 133827 **k** vectors for the low-latitude events detected within 30° from the ecliptic plane. At least 67 **k** vectors were used for the average of each bin. Blanks are due to the lack of observation, the smallness of the number of events, or the inaccuracy of the direction of the **k** vectors.

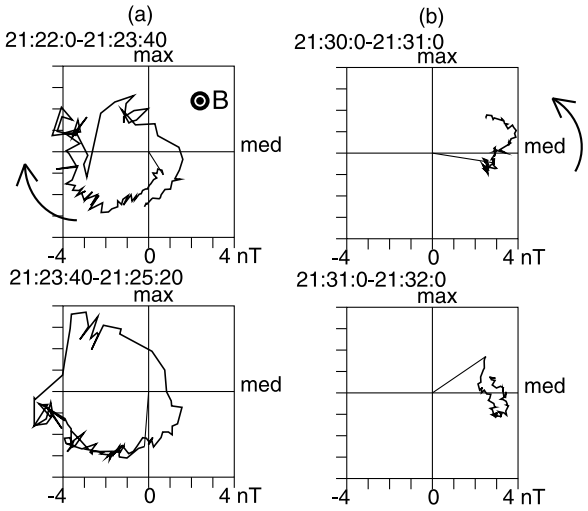

Figure 13. Hodograms of the path of the tip of the magnetic field vector in the plane of maximum and intermediate variance for the periods of (a) 21:21 – 21:25 and (b) 21:30 – 21:34, on 4 January 2008. The hodograms are divided into 2 panels each, so that the direction of rotation would be clear. The minimum variance analysis was applied to longer periods 21:17 – 21:27 for Figure 13a and 21:30 – 21:35 for Figure 13b, producing the minimum variance directions (−0.64, 0.06, 0.77) for Figure 13a and (−0.37, 0.89, 0.27) for Figure 13b. The axes are selected so that the average magnetic field would be directed from the page toward the reader. The short line from the origin of each panel indicates the initial direction of the magnetic field.

the angular frequency matches the proton cyclotron frequency $\Omega_i \equiv qB/m_i$ as

$$\sigma\omega_p' = n\Omega_i \quad (n = 1, 2, 3, \ldots), \tag{6}$$

where q and m_i are the electric charge and the mass of a proton, respectively, and B is the magnitude of the background magnetic field. To check the resonant condition, we need ω and $\mathbf{k}$. The direction of $\mathbf{k}$ is obtained from the minimum variance method. The magnitude $|\mathbf{k}|$ can be derived from the resonant condition as follows. Combining equations (3), (5), and (6) we obtain

$$\omega_{obs} - \sigma\mathbf{k}\cdot\mathbf{V}_p = n\Omega_i, \tag{7}$$

which can be rewritten as

$$|\mathbf{k}| = \frac{-(n\Omega_i - \omega_{obs})}{\sigma|\mathbf{V}_p|\cos\theta_{pk}} \tag{8}$$

using the angle θ_{pk} between the direction of the motion of the reflected proton $\mathbf{V}_p$ and the wave number vector $\mathbf{k}$. The angular frequency ω_{obs} is measurable, and the proton cyclotron frequency Ω_i is calculated from the magnitude B of the magnetic field during the wave activities. The speed of the reflected protons $|\mathbf{V}_p|$ is approximated as nearly equal to the incident solar wind speed $|\mathbf{V}_{sw}|$ according to *Saito et al.* [2008]. We can calculate $|\mathbf{k}|$ from equation (8) if we have the angle θ_{pk}.

[42] Figure 16 shows an example of the estimation of $|\mathbf{k}|$ of the representative event from 21:17 to 21:27 on 4 January 2008, calculated for various θ_{pk} for the $\sigma = 1$ case with $h = 1$ and $\mathbf{B}_0 \cdot \mathbf{k} > 0$. The wave number vector $\mathbf{k}$ was antisunward as the average magnetic field $\mathbf{B}_0$ was directed antisunward during this event. The observed frequency was 0.012 Hz with the left-hand polarization and the proton cyclotron frequency $f_i = \Omega_i/2\pi$ was 0.039 Hz. We employ the fundamental mode $n = 1$ as it is the most important mode. The solar wind speed was 300 km/s. It is recognized in Figure 16a that the wave number $|\mathbf{k}|$ is smallest at $\theta_{pk} = 180°$, while it diverges to infinity as θ_{pk} approaches 90°. Figure 16b shows that the wavelength was about 10^4 km at $\theta_{pk} = 180°$. In the solar wind magnetic field, waves of such wavelength are commonly observed irrespective of the presence of the moon [*e.g.*, *Bruno and Calbone*, 2005, and references therein].

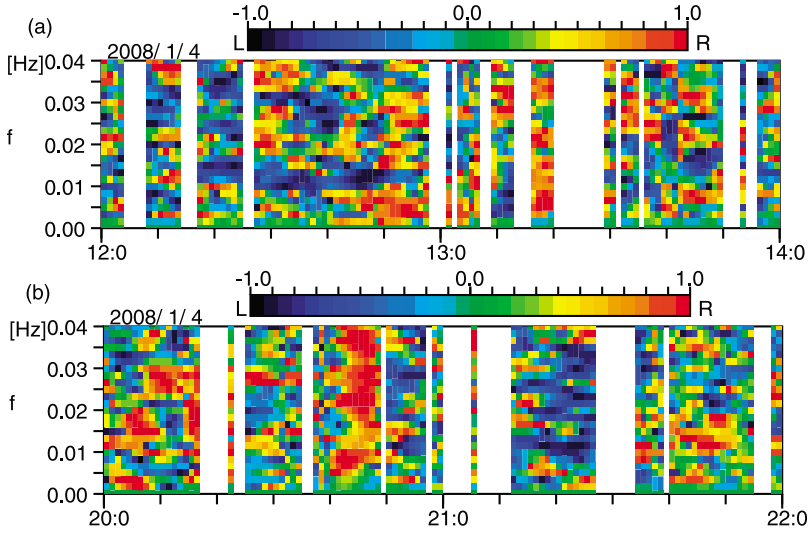

Figure 14. Polarization of each frequency component of the magnetic field variations observed by Kaguya for the same periods displayed in Figure 2. The left (right)-handed polarization is colored with blue(red). The polarization was calculated sliding a 600 s window by 60 s and was displayed at the center of each 600 s period. Blanks are the periods for which the $\mathbf{k}$ vector was not calculated with sufficient accuracy.

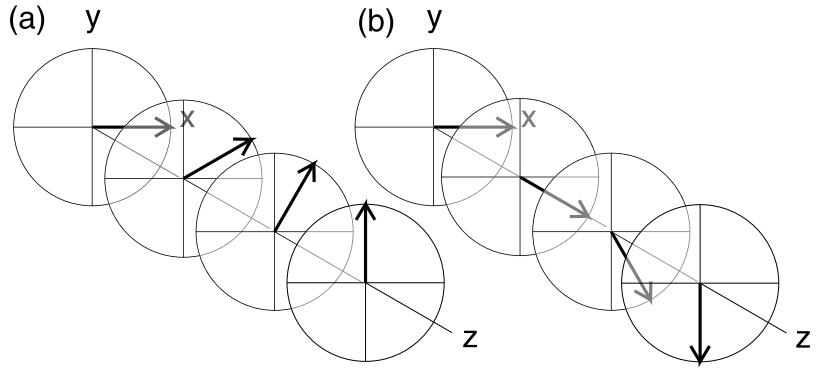

Figure 15. Schematic illustrations of the rotating magnetic field vector **b** given in the form of equation (2) with (a) $h = +1$ and (b) $h = -1$ and positive wave number k.

[43] By substituting the wave number $|\mathbf{k}|$ thus obtained into equation (1), we can calculate the angular frequency ω of the wave in the solar wind frame of reference. Figure 16c shows the frequency $f = \omega/2\pi$. It was negative for all θ_{pk}, indicating that the polarization of the wave was right-handed in the solar wind frame of reference. The negative frequency also implies that the phase velocity $\mathbf{V}_{ph}$ was in the direction opposite to $\mathbf{k}$. The absolute value of the frequency $|f|$ was 5.6×10^{-3} Hz at $\theta_{pk} = 180°$ and lower than the ion cyclotron frequency 0.039 Hz over a wide range of θ_{pk} from 110° to 180°, suggesting that the resonant wave was in the frequency domain of MHD waves. Precisely speaking, they cannot be ideal MHD waves, because the ideal MHD theory predicts linear polarization while they have a distinct elliptical polarization as pointed out by *Russell* [1994a] concerning the upstream waves at the Earth's bow shock.

[44] Figure 16d shows the phase speed $V_{ph} = \omega/|\mathbf{k}|$ which reaches the minimum value 62 km/s at $\theta_{pk} = 180°$. The phase speed of this frequency domain is expected to be of the order of the fast, intermediate, and slow speeds of the MHD waves. The calculated phase speed was much higher than the fast speed $V_f = 30$ km/s of the unperturbed solar wind, indicated with a gray dashed line in Figure 16d, calculated from the upstream solar wind parameters observed by ACE within 3.5 hours of the ULF detection. Using the ion density 5 cm^{-3} and the ion temperature 2×10^4 K, we obtain the Alfvén speed $V_A = 25$ km/s and the sound speed $V_s = 23$ km/s on the assumption of equal temperatures of protons and electrons. As the angle θ_{bk} between $\mathbf{k}$ and the magnetic field was 44°, the fast speed V_f was calculated to be 30 km/s. In order that the fast speed V_f would become 62 km/s, the sound speed V_s needs to be 57 km/s, which requires the proton temperature 1.2×10^5 K, by 6 times as large as the upstream observation. The possibility of the high proton temperature is discussed in the next section.

[45] For the angle θ_{pk} smaller than 180°, the phase speed was too high to be explained with the fast speed V_f. It was also much higher than the phase speed of a whistler wave V_w indicated by the gray solid curve in Figure 16d. It would be natural to think that the most probable angle of θ_{pk} is 180°, indicating that the wave number $\mathbf{k}$ was antiparallel to the velocity $\mathbf{V}_p$ of the reflected protons. Because the angular frequency ω was negative, it implies that the phase velocity was parallel and in the same direction with the velocity of the reflected protons.

[46] The other case of $\sigma = 1$ with $h = -1$ and $\mathbf{B}_0 \cdot \mathbf{k} < 0$ gave physically the same result as that has been described, only with the difference in definition of the axes of the reference frame. The case of $\sigma = -1$ results in the phase speed V_{ph} larger than 190 km/s, which cannot exist in the solar wind plasma of the time of observation.

5. Discussion

[47] As the group velocities of the MHD waves are smaller than the solar wind bulk speed, they cannot propagate against the solar wind flow. The ULF waves detected by Kaguya must

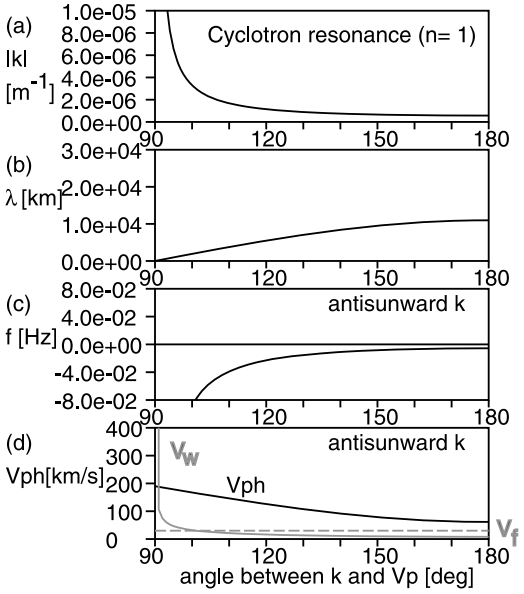

Figure 16. Cyclotron resonance condition calculated for various angles θ_{pk} between the wave number vector $\mathbf{k}$ and the velocity of the reflected protons $\mathbf{V}_p$. From top to bottom: (a) the wave number $|\mathbf{k}|$, (b) the wavelength λ, (c) the frequency f in the solar wind frame calculated on the assumption of antisunward propagation, (d) the phase speed V_{ph} of the wave in the solar wind frame. The gray dashed line and the gray solid curve in Figure 16d indicate the fast mode speed V_f for the temperature 2×10^4 K, and the phase speed V_w of whistler mode wave calculated for each frequency, respectively.

be excited upstream of the spacecraft and then convected down by the solar wind flow, irrespective of the direction of the phase velocity. This mechanism is possible, because the Larmour radius of the reflected protons in the solar wind magnetic field is large. For example, a reflected proton with a speed of 600 km/s relative to the solar wind flow, twice the incident solar wind speed, could have a Larmour radius of 1200 km in a typical magnitude 5 nT of the solar wind magnetic field. Therefore, the reflected proton can travel far upstream and generate a wave. The generated wave could be convected down and then detected by the spacecraft. This process is the same as the upstream waves in the Earth's foreshock [*Fairfield*, 1969, 1974; *Russell*, 1994a, 1994b].

[48] Figure 16 suggests that the resonance condition was satisfied when the **k** vector and the velocity $\mathbf{V}_p$ of the reflected protons were antiparallel to each other. Figures 11c and 12 show that the **k** vectors were statistically nearly perpendicular to the lunar surface just below the observation site. Although the waves are not generated at the surface of the moon, it is suggested that the velocity $\mathbf{V}_p$ of the resonant protons are nearly perpendicular to the lunar surface in the reference frame of the solar wind. Although the protons are not assumed to be reflected specularly at each location of the lunar surface [*Saito et al.*, 2008], it seems natural that the direction of the reflected protons averaged for the broad angular distribution and the wide area is nearly perpendicular to the surface.

[49] Differently from the ULF waves upstream of the Earth's bow shock whose sense of rotation was dominated by the left-hand polarization [*Fairfield*, 1969], only 53% of the monochromatic ULF waves around the moon showed the left-hand polarization. The wave number vector **k** antiparallel to the velocity $\mathbf{V}_p$ of the reflected protons can account for the nearly equal detection of the left-hand and the right-hand polarizations. In case of the Earth's bow shock, the reflection of the solar wind ions is nearly specular [*Gosling and Robson*, 1985]. As the shock surface extends essentially in y and z directions upstream of the Earth, the ions are thought to be reflected into the direction relatively close to the x axis, which makes a small angle with respect to the incident solar wind flow. Thus the contributions from the second and the third terms of equation (4) are nearly the same and much larger than that of the first term. The left-handed wave as seen from the reflected protons is left-handed as well when viewed from the spacecraft. On the other hand, for the event we have seen in Figure 16, the magnitude of the second term $\mathbf{k} \cdot \mathbf{V}_{sw}$ was $2\pi \times 1.7 \times 10^{-2}$ Hz, while that of the third term $\mathbf{k} \cdot \mathbf{V}_p$ was as large as $2\pi \times 2.7 \times 10^{-2}$ Hz. Although the magnitudes of $|\mathbf{k}||\mathbf{V}_{sw}|$ and $|\mathbf{k}||\mathbf{V}_p|$ are nearly the same, the contribution of the second term is smaller than the third term, due to the angle 51° between the wave number vector **k** and the solar wind velocity $\mathbf{V}_{sw}$. Consequently, it can occur that the second term cannot reverse the polarization of ω'_{sc}, resulting in nearly equal opportunity of detection of right-hand and left-hand polarization, while the third term reverses the polarization so that the reflected protons would experience left-hand rotation of the magnetic and the electric fields. Figure 13 shows the examples. The left-handed polarization (Figure 13a) turned to be right-handed (Figure 13b) according as the **k** vector turned from (−0.64, 0.06, 0.77) to (−0.37, 0.89, 0.27), to be less aligned with the solar wind flow.

[50] The dominant frequency 0.01 Hz of the monochromatic ULF waves can be interpreted in terms of the wave number vectors **k** antiparallel to the velocity $\mathbf{V}_p$. Considering $\cos\theta_{pk} = -1$ and ω negligibly small compared with $|\mathbf{k}||\mathbf{V}_{sw}| \sim |\mathbf{k}||\mathbf{V}_p|$, equations (1) and (5) are approximated as

$$\omega'_{sc} \sim |\mathbf{k}||\mathbf{V}_{sw}|\cos\theta_{ks} \tag{9}$$

and

$$\omega'_p \sim |\mathbf{k}||\mathbf{V}_{sw}|(\cos\theta_{ks} + 1), \tag{10}$$

respectively. Eliminating $|\mathbf{k}||\mathbf{V}_{sw}|$ from equations (9) and (10), we have

$$\omega'_{sc} \sim \frac{\cos\theta_{ks}}{\cos\theta_{ks} + 1}\omega'_p \tag{11}$$

which is rewritten as

$$\omega_{obs} \sim \frac{\cos\theta_{ks}}{\cos\theta_{ks} + 1} n\Omega_i \tag{12}$$

using equations (3) and (6). Substituting $n = 1$ and $\Omega_i \sim 0.48$ rad/s for the typical solar wind magnetic field $B_0 \sim 5$ nT, we have $\omega_{obs} \sim 0.06$ rad/s, that is, 0.01 Hz, if the angle θ_{ks} is ±80°. The wave propagation into such directions $\theta_{ks} = \pm 80°$ were observed at the terminator, the site of the highest occurrence rate of the ULF wave. On the other hand, at present it is not known why the occurrence rate of the ULF waves was high at around the terminator.

[51] The high proton temperature required for the phase speed 62 km/s can be explained with the sum of the kinetic energy of the reflected protons. If we assume that 1% of the solar wind protons were reflected by the moon [*Saito et al.*, 2008], their contribution to the ion thermal energy of the solar wind would be $0.01 N_i m_i (\mathbf{V}_p - \mathbf{V}_{sw})^2/2 \sim 1.5 \times 10^{-11}\mathrm{Jm}^{-3}$ on a very rough estimation of $|\mathbf{V}_p - \mathbf{V}_{sw}| \sim 2|\mathbf{V}_{sw}|$, where N_i is the number density of the solar wind protons. The speed $|\mathbf{V}_{sw}|$ of the solar wind flow was about 300 km/s at the time corresponding to the detection of the ULF wave. The sum of the energy of the reflected protons is about 6.8 times as large as the thermal energy $N_i m_i V_s^2/2 \sim 2.2 \times 10^{-12}\mathrm{Jm}^{-3}$ of the upstream solar wind. This is just rough estimation, because it is not likely that the reflected protons were collimated in the direction antiparallel to the incident velocity. Rather, it is likely that pitch angle scattering of the reflected protons is caused by the large amplitude ULF waves [*Gary et al.*, 1984b].

[52] The sum of the kinetic energy of the reflected protons can account for the energy density of the monochromatic ULF waves, $3.6 \times 10^{-12}\mathrm{Jm}^{-3}$ at most, calculated from the largest amplitude of the ULF waves of 3 nT as seen in Figures 1 and 4. It suggests that the energy of the reflected protons is the source of the energy of the ULF waves.

[53] The monochromatic ULF waves were often accompanied with the non-monochromatic, higher-frequency whistlers which were almost always detected above the dayside surface of the moon in the solar wind [*Nakagawa et al.*, 2011]. The both modes were observed simultaneously in many cases, while occasionally they were detected with the absence of another. The situation is the same as that of the Earth's foreshock region, where large amplitude low-frequency waves from 0.01 to 0.05 Hz and higher-frequency of 0.5 – 4 Hz are observed [*e.g.*, *Fairfield*, 1974; *Hoppe et al.*, 1981; *Russell*, 1994a, 1994b, and references therein]. The two modes were

often accompanied with backstreaming ions from the bow shock. *Hoppe et al.*[1981] showed that the higher frequency waves were accompanied with cold beam ions, while the low frequency waves were associated with diffuse ions with a broad energy spectrum. The upstream waves associated with the backscattered ions have motivated many theoretical and numerical works on the wave generation by the ion beam. *Gary et al.* [1981, 1984a, 1984b] studied the ion beam instability using the Vlasov theory and showed that the maximum growth rate is found at the direction parallel to the magnetic field, while a significant growth rate is also found at an oblique angle. It seems to be in good accordance with the propagation property of the ULF waves in the present study. Using the reflected ion component backstreaming along the magnetic field, *Winske and Leroy* [1984] found that diffuse ion distributions are produced as the wave grows. It was also shown that ring beam ions generate high frequency waves as well as low frequency resonant mode waves [*Winske et al.*, 1985; *Wong and Goldstein*, 1987]. *Gurgiolo et al.* [1993] showed that gyrophase bunched ions reflected at the shock generate both low and high frequency waves with timescales much shorter than gyrophase mixing, and the low frequency waves trap the phase bunched ions and prevent them from the phase mixing. It is likely that the protons reflected by the moon form a ring beam. On the basis of Nozomi observation, *Futaana et al.* [2003] showed that the nonthermal protons coming from the dayside surface of the moon had a ring beam distributions. In the vicinity of a significant crustal magnetic field, phase bunched protons may also be expected.

6. Conclusion

[54] The large amplitude, monochromatic ULF waves of the frequency of 0.01 Hz were detected by Kaguya around the moon. They were thought to be generated by the solar wind protons reflected by the moon through the cyclotron resonance with the MHD waves in the solar wind plasma. The direction of propagation was not always parallel to the solar wind magnetic field, but showed preference to the directions parallel to the magnetic field and perpendicular to the lunar surface below the spacecraft. The direction of propagation of the wave is thought to be parallel to the reflected protons, while the angle between the solar wind flow and the wave propagation was large. It can account for the observed frequency about 0.01 Hz. The estimated phase speed was higher than the fast mode speed of the unperturbed, upstream solar wind, but can be accounted for if the thermal effect of the reflected protons is taken into account.

[55] **Acknowledgments.** The authors thank the Kaguya MAP/LMAG team for the Kaguya magnetic field observations. We thank the ACE MAG instrument team, the ACE SWEPAM instrument team and the ACE Science Center for providing the ACE data. This study was supported by the JSPS grant-in-aid for scientific research project 21540461 and in part by Grant for Basic Science Research Projects from the Sumitomo Foundation.

[56] Masaki Fujimoto thanks the reviewers for their assistance in evaluating this paper.

References

Bosqued, J. M., et al. (1996), Moon-solar wind interaction: First results from the WIND/3DP experiment, *Geophys. Res. Lett.*, *23*, 1259–1262.

Bruno, R. and V. Carbone (2005), The solar wind as a turbulent laboratory, *Living Rev. Solar Phys.*, *2*, lrsp-2005-4.

Colburn, D. S., R. G. Currie, J. D. Mihalov, and C. P. Sonett (1967), Diamagnetic solar-wind cavity discovered behind Moon, *Science*, *158*, 1040–1042.

Colwell, J. E., S. Batiste, M. Horányi, S. Robertson, and S. Sture (2007), Lunar surface: Dust dynamics and regolith mechanics, *Rev. Geophys.*, *45*, RG2006, doi:10.1029/2005RG000184.

Fairfield, D. H. (1969), Bow shock associated waves observed in the far upstream interplanetary medium, *J. Geophys. Res.*, *74*, 3541–3553.

Fairfield, D. H. (1974), Whistler waves observed upstream from collisionless shocks, *J. Geophys. Res.*, *79*, 1368–1378.

Farrell, W. M., R. J. Fitzenreiter, C. J. Owen, J. B. Byrnes, R. P. Lepping, K. W. Ogilvie, and F. Neubauer (1996), Upstream ULF waves and energetic electrons associated with the lunar wake: Detection of precursor activity, *Geophys. Res. Lett.*, *23*, 1271–1274.

Freeman, J. W., and M. I. Ibrahim (1975), Lunar electric fields, surface potential and associated plasma sheaths, *Moon*, *14*, 103–114.

Freeman, J. W., Jr., M. A. Fenner, and H. K. Hills (1973), Electric potential of the moon in the solar wind, *J. Geophys. Res.*, *78*, 4560–4567.

Futaana, Y., S. Machida, Y. Saito, A. Matsuoka, and H. Hayakawa (2001), Counterstreaming electrons in the near vicinity of the moon observed by plasma instruments on board NOZOMI, *J. Geophys. Res.*, *106*, 18,729–18,740.

Futaana, Y., S. Machida, Y. Saito, A. Matsuoka, and H. Hayakawa (2003), Moon-related nonthermal ions observed by NOZOMI: Species, sources, and generation mechanisms, *J. Geophys. Res.*, *108*(A1), 1025, doi:10.1029/2002JA009366.

Gary, S. P., J. T. Gosling, and D. W. Forslund (1981), The electromagnetic ion beam instability upstream of the Earth's bow shock, *J. Geophys. Res.*, *86*, 6691–6696.

Gary, S. P., J. T. Gosling, and D. W. Forslund (1984a), Correction to "The electromagnetic ion beam instability upstream of the Earth's bow shock," *J. Geophys. Res.*, *89*, 404.

Gary, S. P., C. W. Smith, M. A. Lee, M. Goldstein, and D. W. Forslund (1984b), Electromagnetic ion beam instabilities, *Phys. Fluids*, *27*(7), 1852–1862.

Gosling, J. T., and A. E. Robson (1985), Ion reflection, gyration, and dissipation at supercritical shocks, in *Collisionless Shocks in the Heliosphere: Reviews of Current Research*, *Geophys. Monogr. Ser.*, vol. 35, edited by B. T. Tsurutani and R. G. Stone, pp. 141–152, AGU, Washington, D. C., doi:10.1029/GM035p0141.

Gurgiolo, C., H. K. Wong, and D. Winske (1993), Low and high frequency waves generated by gyrophase bunched ions at oblique shocks, *Geophys. Res. Lett.*, *20*(9), 783–786.

Greenstadt, E. W., G. Le, and R. T. Strangeway (1995), ULF waves in the foreshock, *Adv. Space Res.*, *15*(8–9), 71–84.

Halekas, J. S., D. L. Mitchell, R. P. Lin, L. L. Hood, M. N. Acu na, and A. B. Binder (2002), Evidence for negative charging of the lunar surface in shadow, *Geophys. Res. Lett.*, *29*(10), 1435, doi:10.1029/2001GL014428.

Halekas, J. S., R. P. Lin, and D. L. Mitchell (2003), Inferring the scale height of the lunar nightside double layer, *Geophys. Res. Lett.*, *30*(21), 2117, doi:10.1029/2003GL018421.

Halekas, J. S., S. D. Bale, D. L. Mitchell, and R. P. Lin (2005), Electrons and magnetic fields in the lunar plasma wake, *J. Geophys. Res.*, *110*, A07222, doi:10.1029/2004JA010991.

Halekas, J. S., D. A. Brain, D. L. Mitchell, R. P. Lin, and L. Harrison (2006a), On the occurrence of magnetic enhancements caused by solar wind interaction with lunar crustal fields, *Geophys. Res. Lett.*, *33*, L08106, doi:10.1029/2006GL025931.

Halekas, J. S., D. A. Brain, D. L. Mitchell, and R. P. Lin (2006b), Whistler waves observed near lunar crustal magnetic sources, *Geophys. Res. Lett.*, *33*, L22104, doi:10.1029/2006GL027684.

Halekas, J. S., G. T. Delory, R. P. Lin, T. J. Stubbs, and W. M. Farrell (2008), Lunar Prospector observations of the electrostatic potential of the lunar surface and its response to incident currents, *J. Geophys. Res.*, *113*, A09102, doi:10.1029/2008JA013194.

Hoppe, M. M., C. T. Russell, L. A. Frank, T. E. Eastman, and E. W. Greenstadt (1981), Upstream hydromagnetic waves and their association with backstreaming ion populations: ISEE 1 and 2 Observations, *J. Geophys. Res.*, *86*, 4471–4492, doi:10.1029/JA086iA06p04471.

Kellogg, P. J., K. Goetz, and S. J. Monson (1996), Observation of lunar plasma waves during a travel of the Moon's wake, *Geophys. Res. Lett.*, *23*, 1267–1270.

Le, G., and C. T. Russell (1992), Study of ULF wave foreshock morphology-I: ULF foreshock boundary, *Planet. Space Sci.*, *40*, 1203–1213.

Lepping, R. P., and W. Behannon (1980), Magnetic field directional discontinuities: 1. Minimum variance errors, *J. Geophys. Res.*, *85*, 4695–4703.

Lin, R. P., D. L. Mitchell, D. W. Curtis, K. A. Anderson, C. W. Carlson, J. McFadden, M. H. Acu na, L. L. Hood, and A. Binder (1998), Lunar surface magnetic fields and their interaction with the solar wind: Results from Lunar Prospector, *Science*, *281*, 1480–1484.

Lindeman, R., J. W. Freeman Jr., and R. R. Vondrak (1973), Ions from the lunar atmosphere, *Geochim. Cosmochim. Acta*, *3*, 2889–2896.

LRO Project and LGCWG (2008), A Standardized Lunar Coordinate System for the Lunar Reconnaissance Orbiter and Lunar Datasets, *White Pap. Version 5*, 13 pp., Goddard Space Flight Cent., Greenbelt, Md.

Lue, C., Y. Futaana, S. Barabash, M. Wieser, M. Holmström, A. Bhardwaj, M. B. Dhanya, and P. Wurz (2011), Strong influence of lunar crustal fields on the solar wind flow, *Geophys. Res. Lett.*, *38*, L03202, doi:10.1029/2010GL046215.

Lyon, E. F., H. S. Bridge, and J. H. Binsak (1967), Explorer 35 plasma measurements in the vicinity of the Moon, *J. Geophys. Res.*, *72*, 6113–6117.

Mitchell, D. L., J. S. Halekas, R. P. Lin, S. Frey, L. L. Hood, M. H. Acu na, and A. Binder (2008), Global mapping of lunar crustal magnetic fields by Lunar Prospector, *Icarus*, *194*(2), 401–409.

Nakagawa, T., Y. Takahashi, and M. Iizima (2003), GEOTAIL observation of upstream ULF waves associated with lunar wake, *Earth Planets Space*, *55*, 569–580.

Nakagawa, T., F. Takahashi, H. Tsunakawa, H. Shibuya, H. Shimizu, and M. Matsushima (2011), Non-monochromatic whistler waves detected by Kaguya on the dayside surface of the Moon, *Earth Planets Space*, *63*, 37–46.

Ness, N. F., K. W. Behannon, H. E. Taylor, and Y. C. Whang (1968), Perturbations of the interplanetary magnetic field by the lunar wake, *J. Geophys. Res.*, *73*, 3421–3440.

Nishino, M. N., et al. (2009), Solar-wind proton access deep into the near-Moon wake, *Geophys. Res. Lett.*, *36*, L16103, doi:10.1029/2009GL039444.

Ogilvie, K. W., J. T. Steinberg, R. T. Fitzenreiter, C. J. Owen, A. J. Lazarus, W. M. Farrell, and R. B. Torbert (1996), Observation of the lunar plasma wake from the WIND spacecraft on December 27, 1994, *Geophys. Res. Lett.*, *23*, 1255–1258.

Owen, C. J., R. P. Lepping, K. W. Ogilvie, J. A. Slavin, W. M. Farrell, and J. B. Byrnes (1996), The lunar wake at 6.8 R_L: WIND magnetic field observations, *Geophys. Res. Lett.*, *23*, 1263–1266.

Purucker, M. E., and J. B. Nicholas (2010), Global spherical harmonic models of the internal magnetic field of the Moon based on sequential and coestimation approaches, *J. Geophys. Res.*, *115*, E12007, doi:10.1029/2010JE003650.

Richmond, N. C., and L. L. Hood (2008), A preliminary global map of the vector lunar crustal magnetic field based on Lunar Prospector magnetometer data, *J. Geophys. Res.*, *113*, E02010, doi:10.1029/2007JE002933.

Russell, C. T. (1994a), Planetary upstream waves, in *Solar Wind Sources of Magnetospheric Ultra-Low-Frequency Waves*, *Geophys. Monogr. Ser.*, vol. 81, edited by M. J. Engebretson, K. Takahashi, and M. Scholer, pp. 75–86, AGU, Washington, D. C.

Russell, C. T. (1994b), Magnetospheric and solar wind studies with co-orbiting spacecraft, in *Solar System Plasmas in Space and Time*, *Geophys. Monogr. Ser.*, vol. 84, edited by J. L. Burch and J. H. Waite Jr., pp. 85–100, AGU, Washington, D. C.

Russell, C. T., and B. R. Lichtenstein (1975), On the source of lunar limb compressions, *J. Geophys. Res.*, *80*, 4700–4711.

Saito, Y., et al. (2008), Solar wind proton reflection at the lunar surface: Low energy ion measurement by MAP-PACE onboard SELENE (Kaguya), *Geophys. Res. Lett.*, *35*, L24205, doi:10.1029/2008GL036077.

Saito, Y., et al. (2010), In-flight performance and initial results of Plasma energy Angle and Composition Experiment (PACE) on SELENE (Kaguya), *Space Sci. Rev.*, *154*, 265–303, doi:10.1007/s11214–010–9647–x.

Schubert, G., and B. R. Lichtenstein (1974), Observations of moon-plasma interactions by orbital and surface experiments, *Rev. Geophys.*, *12*, 592–626.

Shimizu, H., F. Takahashi, N. Horii, A. Matsuoka, M. Matsushima, H. Shibuya, and H. Tsunakawa (2008), Ground calibration of the high-sensitivity SELENE lunar magnetometer LMAG, *Earth Planets Space*, *60*, 353–363.

Sonnerup, B. U. Ö., and L. J. Cahill Jr. (1967), Magnetopause structure and attitude from Explorer 12 observations, *J. Geophys. Res.*, *72*, 171–183.

Sugiyama, T., T. Terasawa, H. Kawano, T. Yamamoto, S. Kokubun, L. A. Frank, K. Ackerson, and B. T. Tsurutani (1995), Attenuation distance of low frequency waves upstream of the pre-dawn bow shock: GEOTAIL and ISEE 3 comparison, *Geophys. Res. Lett.*, *22*, 81–84.

Takahashi, F., H. Shimizu, M. Matsushima, H. Shibuya, A. Matsuoka, S. Nakazawa, Y. Iijima, H. Otake, and H. Tsunakawa (2009), In-orbit calibration of the lunar magnetometer onboard SELENE (KAGUYA), *Earth Planets Space*, *61*, 1269–1274.

Tsunakawa, H., H. Shibuya, F. Takahashi, H. Shimizu, M. Matsushima, A. Matsuoka, S. Nakazawa, H. Otake, and Y. Iijima (2010), Lunar magnetic field observation and initial global mapping of lunar magnetic anomalies by MAP-LMAG onboard SELENE (Kaguya), *Space Sci. Rev.*, *154*, 219–251, doi:10.1007/s11214–010–9652–0.

Wang, X.-D., et al. (2010), Acceleration of scattered solar wind protons at the polar terminator of the Moon: Results from Chang'E-1/SWIDs, *Geophys. Res. Lett.*, *37*, L07203, doi:10.1029/2010GL042891.

Winske, D., and M. M. Leroy (1984), Diffuse ions produced by electromagnetic ion beam instabilities, *J. Geophys. Res.*, *89*, 2673–2688.

Winske, D., C. S. Wu, Y. Y. Li, Z. Z. Mou, and S. Y. Guo (1985), Coupling of newborn ions to the solar wind by electromagnetic instabilities and their interaction with the bow shock, *J. Geophys. Res.*, *90*, 2713–2726.

Wong, H. K., and M. L. Goldstein (1987), Proton beam generation of whistler waves in the Earth's foreshock, *J. Geophys. Res.*, *92*, 12,419–12,424, doi:10.1029/JA092iA11p12419.

M. Matsushima, F. Takahashi, and H. Tsunakawa, Department of Earth and Planetary Sciences, Tokyo Institute of Technology, 2-12-1 Ookayama, Meguro-ku, Tokyo 152-8551, Japan.

T. Nakagawa and A. Nakayama, Information and Communication Engineering, Tohoku Institute of Technology, 35-1, Kasumicho, Yagiyama, Taihaku-ku, Sendai, Miyagi 982-8577, Japan. (nakagawa@tohtech.ac.jp)

H. Shibuya, Department of Earth and Environmental Sciences, Kumamoto University, 39-1, Kurokami 2-chome, Kumamoto 860-8555, Japan.

H. Shimizu, Earthquake Research Institute, University of Tokyo, 1-1-1, Yayoi, Bunkyo-ku, Tokyo 113-0032, Japan.

Erratum

In the originally published version of this article, the power of lowest and second lowest frequencies displayed in Figures 2 and 5 were incorrect. This error has since been corrected, and this version may be considered the authoritative version of record.

Figure 2.

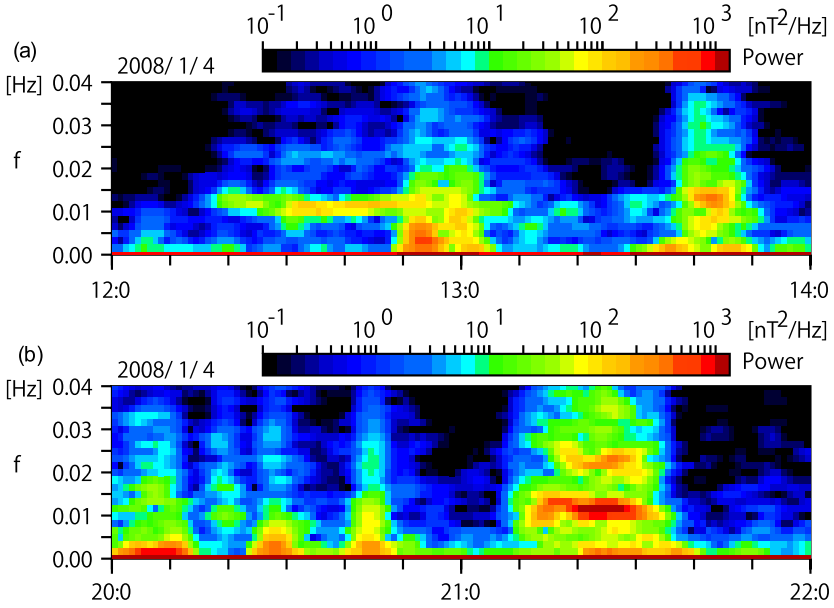

Figure 5.